DESIGN AND EXPERIMENT OF COMBINED AXIAL-FLOW CORN PLOT THRESHING DEVICE
/
组合轴流式玉米小区脱粒装置设计与实验

Long-yuan ZHANG[1)], Xiao-wei GE[2)], Jun-nan LI[1)], Chen WANG[1)] Xiang-kun LI[1)], Guo-liang LI*[)]
[1)] College of Mechanical and Electrical Engineering, Qingdao Agricultural University, Qingdao / China
[2)] Qingdao Plantech Machinery Technology Co., Ltd, Qingdao / China
Tel: +86 13156058765; E-mail: lglplantech@126.com
Corresponding author: Guo-liang LI
DOI: https://doi.org/10.35633/inmateh-78-08

Keywords: *corn threshing, axial flow drum, rod-tooth and spike-tooth combination, response surface optimization*

ABSTRACT
In order to address the challenges associated with wide moisture content variation in corn ears, significant operational fluctuations, and stringent kernel damage control requirements during threshing in experimental plots, a combined rod-tooth and spike-tooth axial-flow corn threshing device was designed. Based on the movement and force characteristics of the cobs during the axial-flow threshing process, the key component parameters of the machine such as the threshing drum, concave screen and flow guide structure were calculated and designed, and the three-dimensional model of the whole machine was built. Taking the discrete element method, the movement behavior of ears in the threshing drum was simulated and analyzed, and the influence of the combined threshing components on the axial transport characteristics of ears was focused on. At the same time, modal analysis of threshing drum was conducted by finite element method, and structural dynamic safety in operation speed range was verified. A multi-factor experiment was carried out on combined axial-flow corn threshing test bench, taking drum speed, feed rate and threshing gap as experimental factors and kernel breakage rate and unthreshed kernel rate as evaluation indexes. In this study, Design-Expert software was used to analyze the experimental results and optimize the parameters. Multi-objective optimization identified an optimal parameter combination with a drum speed of approximately 339 r/min, a feed rate of about 3.6 kg/s, and a threshing gap of around 45 mm. Field validation results showed good agreement with the model predictions, indicating that the combined axial-flow threshing device meets the operational requirements of small plots and exhibits good adaptability and operational stability.

摘要
针对玉米试验小区脱粒作业中果穗含水率分布范围宽、作业工况波动大且籽粒损伤控制要求高的问题，设计了一种杆齿—钉齿组合式轴流玉米脱粒装置。依据轴流脱粒过程中果穗运动与受力特征，对脱粒滚筒、凹板筛及导流结构等关键部件参数进行了设计计算，并建立了整机三维模型。通过离散元方法对果穗在脱粒滚筒内的运动行为进行仿真分析，重点研究组合脱粒元件对果穗轴向输送特性的影响；同时，采用有限元方法对脱粒滚筒进行模态分析，验证其在工作转速范围内的结构动态安全性。以滚筒转速、喂入量和脱粒间隙为试验因素，以籽粒破碎率和未脱净率为评价指标，在组合轴流式玉米脱粒试验台上开展多因素试验研究，并利用 Design-Expert 软件对试验结果进行分析与参数优化。经多目标优化得到较优作业参数组合为：滚筒转速约 339 r/min、喂入量约 3.6 kg/s、脱粒间隙约 45 mm。田间验证试验结果与模型预测值吻合较好，表明该组合式轴流脱粒装置在小区作业条件下具有良好的适应性与作业稳定性。

INTRODUCTION
During corn harvesting, the degree of kernel damage during the threshing process has a significant impact on threshing quality. Especially under conditions of high kernel moisture content or large differences in ear size, the impact and compressive forces generated during threshing can easily cause kernel breakage, husk damage, and latent damage, thereby affecting the accuracy of yield measurement and kernel quality (*Chen., 2024; Xin et al., 2024*).

[1] *Longyuan Zhang, M.S. Eng.; Xiaowei Ge, Engineer; Junnan Li, M.S. Eng.; Chen Wang, M.S. Eng.; Xiangkun Li, M.S. Eng.; Guoliang Li, Senior Engineer.*

At present, the structural configuration and parameter settings of corn threshing devices are mainly designed for large-scale field operations. Their design objectives focus on operational efficiency and processing capacity and, to some extent, rely on uniform crop characteristics and stable operating conditions.

Compared to large-scale field harvesting, corn test plots exhibit significant differences in both the objects and conditions of the operation. These plots usually have many different varieties and treatment combinations, inconsistent maturity of ears, a wide range of kernel moisture content distribution, and small and often changing batch sizes. Under such circumstances, if the threshing intensity is maintained at a high level in the initial stage of processing, it will put excessive instantaneous load on the high-moisture ears, thereby increasing the rate of damage to the kernels. On the contrary, simply reducing the drum speed or widening the threshing gap may result in incomplete threshing, which will affect the percentage of unthreshed kernels and the reliability of the yield measurement data. Therefore, the requirements for threshing equipment in terms of low damage, stability and adaptability to ears of different moisture contents in corn plot threshing operations are relatively high (*Shi et al., 2025; Yuan et al., 2024*).

It is found from the current research results that corn kernels fall off the cob is not in one step, but a step-by-step process of loosening to the final complete falling off. The required form and intensity of action from threshing parts differ in these stages, and scholars at home and abroad have carried out systematic studies on the structures of threshing parts and their parameter matching relationships (*Abdeen et al., 2021; Zhao et al., 2024; Steponavičius et al., 2023*). Different threshing mechanism, such as ribbed bar, spike tooth and plate tooth, respectively have different advantages in reducing kernel damage or improving complete threshing effect. The longitudinal axial-flow threshing device extends the residence time of materials in the drum, enhances threshing and separation efficiency, and has been widely applied in corn harvesting machinery (*Wang et al., 2021; Mousaviraad and Tekeste, 2020; Vlăduț et al., 2022, 2023*). Most existing studies focus on reasonably controlling the degree of threshing and optimizing the axial flow movement of materials as effective methods to reduce threshing damage (*Srison et al., 2016; Chen et al., 2021; Xing et al., 2024*).

Given the wide range of moisture content of corn ears during the harvest test and the high accuracy requirements for threshing and yield measurement, this study uses freshly harvested corn ears of the variety Xianyu 335 as the experimental material and proposes a combined axial-flow threshing structure of rod-tooth and spike-tooth types. The threshing elements with different modes of action are segmentally arranged in the axial direction of the drum, and the cob is subjected to a primary initial threshing followed by a secondary stage dominated by rubbing and supplementary threshing. Experimental studies were conducted on the effects of threshing component structural parameters, concave-screen matching relationships, and operational parameters on threshing performance and axial motion characteristics.

MATERIALS AND METHODS

Structure and Working Process of the Combined Axial-Flow Threshing Machine

The test bench of the combined axial-flow threshing device, as shown in Fig.1, mainly consists of an outer frame, a combined axial-flow threshing drum, concave sieves, an upper guide cover plate, a transmission system and walking support components. The entire machine uses a three-phase asynchronous motor as the power source, which is connected to the drum via a cross-shaft universal joint to ensure smooth power transmission and speed adjustment. The grouped concave sieves are arranged below the threshing drum and, together with the drum, form the threshing and separation chamber. Spiral guide plates are installed on the inner surface of the upper guide cover plate to guide the stable axial movement of corn ears within the drum *(Di et al., 2018; Shi, 2018)*.

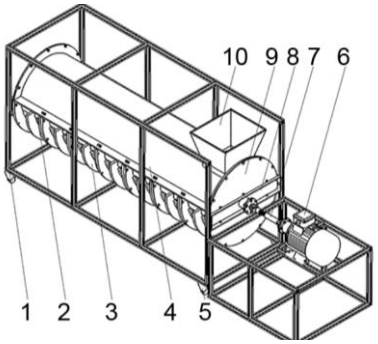

Fig. 1 - Overall structural diagram of combined axial-flow threshing unit

1. Outer frame; 2. Combined axial-flow threshing drum; 3. Concave plate screen; 4. Upper guide cover plate; 5. Casters; 6. Three-phase asynchronous motor; 7. Cross-shaft universal joint; 8. Fixed plate; 9. End plate; 10. Feed inlet.

The test bench was designed based on the principles of axial feeding and staged threshing. The axial conveyance of corn ears by the rotating drum is continuous, gradually completing the threshing and separation processes. During operation, corn ears enter the threshing unit through the feed inlet and move axially under the action of the spiral deflector. They first enter the rod-tooth section, where the first braking action is formed. In this stage, the threshing intensity is relatively low, allowing the kernels to be gradually loosened and initial kernel separation to occur. The separated kernels are intercepted by the concave plate screen, preventing repeated stress within the threshing area.

As the material continues to move forward, partially threshed cobs enter the spike-tooth section. In this region, the cobs are scrubbed and compressed against the concave screen to remove the remaining kernels. Most of the separation occurs during the initial stage; therefore, the material entering the later stage mainly consists of loose kernels and cobs. In this way, the application of high-intensity concentrated forces on intact ears is effectively avoided, thereby reducing the risk of kernel breakage. After threshing, cobs and light impurities are discharged from the threshing area by the axial thrust generated by the axial arrangement of the drum elements, and the kernels and impurities are fully separated.

Combined Threshing Device Design and Mechanism Analysis

Threshing Drum Design

The threshing drum is an important part of the threshing and conveying process in the combined axial-flow corn threshing device. Its structural configuration and parameter setting directly affect the threshing thoroughness and the stress state of the threshed kernels. In view of the characteristics of the experimental corn ears with significant changes in moisture content and the strict requirements for reducing kernel damage during threshing, this study adopts a combination configuration composed of open bar teeth section and closed spike teeth section arranged axially in series. This design can achieve a gradual shift from the initial stage to the fine threshing stage during the process.

The total length of the preliminary design specifications of the threshing drum is 1 800 mm, the main shaft diameter is 76 mm, and the reduced diameter of 64 mm at both ends is used to fit the universal joint coupling. The rod-tooth and spike-tooth parts are arranged axially, with the rod-tooth part being 1 200 mm and the spike-tooth part being 600 mm. This proportional configuration can ensure that the ears are sufficient orientation adjustment and preliminary threshing in front of entering a high-intensity threshing zone to reduce kernel breakage caused by force concentration in the following stage.

When determining the drum length, both the design feed rate and the unit-length threshing capacity of the axial-flow threshing unit should be considered. According to relevant design principles provided in agricultural machinery design handbooks, the drum length can be calculated using Eq. (1):

$$L \geq \frac{Q}{q} \tag{1}$$

where Q is the design feed rate kg/s and q is the threshing capacity per unit length kg/(s·m). Based on the structure of the corn ear and the flow characteristics of the crop, q is taken as 2.2-2.5 kg/(s·m). When Q is set between 4 and 5 kg/s, the calculated value of the drum length is about 1.6-2.0 m, taking into account the threshing stroke, structure layout and overall size of the test bench, the final length of the drum is determined to be 1.8 m.

To determine the working outer diameter of the drum, both the threshing space and the ranges of rotational speed and power consumption should be considered. Based on common design practices for axial-flow threshing units, the working outer diameter can be determined using Eq. (2):

$$D_w = D_b + 2h \tag{2}$$

where D_W is the working outer diameter, D_b is the root circle diameter (360 mm in this study), and h is the height of the threshing elements (70 mm in this study). The calculation results in a working outer diameter of D_W = 500 mm. This dimension reduces reliance on high rotational speed and provides sufficient threshing space, thereby enabling better control of kernel damage.

Threshing capacity of axial - flow threshing drums is closely related to drum linear velocity *(Li et al., 2024)*. According to relevant research and engineering experience, the appropriate drum linear velocity for corn threshing is generally 7 to 9 m/s. The relationship among drum linear velocity, rotational speed, and working outer diameter is given by Eq. (3):

$$v = \frac{\pi D n}{60} \tag{3}$$

where *v* is the drum linear velocity (m/s); *D* is the working outer diameter (mm); *n* is the drum rotational speed (r/min). In this study, the working outer diameter of the drum was 500 mm. When the drum rotational speed n ranged from 250 to 350 r/min, the corresponding linear velocity ranged from 6.5 to 9.2 m/s. This range covers the recommended linear velocity for corn threshing, achieving effective threshing while avoiding excessive kernel breakage caused by overly high linear velocity.

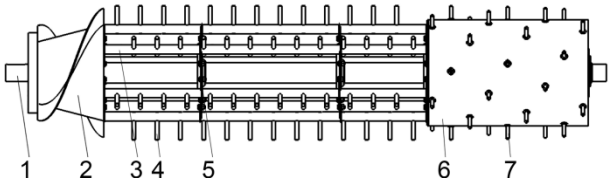

Fig. 2 - Combined axial-flow threshing drum
1. Threshing drum main shaft; 2. Screw feeder; 3. Rod-tooth connecting pipe; 4. Rod teeth; 5. End plate; 6. Spike-tooth section drum; 7. Spike teeth.

Analysis of the Working Mechanism of Threshing Components

This study adopts a threshing structure that combines rod-tooth and spike-tooth sections connected in series. When corn ears enter the threshing chamber, they initially maintain high structural integrity, and the kernels are tightly attached to the cob. Agitation and tumbling actions are required to disrupt the ear structure. As threshing progresses and the ears become loosened, the kernels are gradually separated and discharged, which enhances threshing cleanliness and reduces kernel damage.

The rod-tooth section is located at the front of the threshing drum and mainly responsible for the first threshing and axial conveying. The rod teeth are arranged in a helical staggered pattern along the surface of the drum. During the rotation of the drum, the rod teeth periodically pull and toss the ears, making them flip radially and gradually having an axial movement tendency, at this time the ears have not yet been fully loosened, so the rod teeth are collectively inclined at 20 ° toward the direction of rotation of the drum. This forms a "dragging" effect on top of impact and agitation, helping to reduce ear stagnation in the bottom area and guide continuous axial advancement.

To describe the influence of the spiral arrangement on axial conveying characteristics, a spiral conveying model was introduced in the structural design. The axial material conveying velocity is given by Eq.(4):

$$V_a = \frac{P \cdot n}{60} \tag{4}$$

The spike-tooth section is located at the rear of the threshing drum and is mainly used for kneading and secondary threshing. Compared with rod teeth, spike teeth provide more concentrated contact with the ears, making it easier to achieve stable pressing and kneading at the same rotational speed and thereby further separate unthreshed kernels. At the same time, the axial helical arrangement of the spike teeth continuously applies axial force to the ears and conveys them toward the discharge end, reducing material retention within the threshing chamber.

Fig. 3 - Axial velocity distribution map from the EDEM simulation

Numerical simulation of ear movement within the threshing drum was conducted using the discrete element method. The axial velocity component of the ear center of mass was selected as the evaluation index to analyze the axial motion characteristics. The simulation results indicate significant variations in axial velocity within the rod-tooth section, with short-term back-and-forth oscillations occurring at certain moments; however, the overall rearward conveying trend is maintained. Upon entering the spike-tooth section, axial velocity fluctuations are significantly reduced and the motion becomes more stable. The structural differences and force application characteristics between the two threshing sections gradually promote stable axial advancement of the cob, ensuring continuous threshing *(Zhang et al., 2025)*.

Concave Screen and Upper Guide Cover Plate Design

In the combined axial-flow threshing device, the concave plate screen and the upper guide cover plate together form the primary constraint and guiding boundaries for corn ears within the drum. Their structural configuration and parameter matching have a significant influence on material motion within the threshing channel, separation efficiency, and the likelihood of blockage, distinguishing this system from configurations composed solely of threshing elements. In this structural system, the concave screen and upper guide cover plate mainly control the movement path and force environment acting on the cobs, which is critical for maintaining continuous axial threshing.

Taking advantage of the axial arrangement of the spiral feeder, rod-tooth section, and spike-tooth section, the concave plate screen adopts a segmented axial straight-bar structure to meet the different constraint and separation intensity requirements under various threshing conditions. The concave plate screen is composed of 27 circular steel bars, each with a diameter of 16 mm. The screen panels subtend an angle of 180°, forming a stable threshing and separation area beneath the drum. Along the axial direction, the concave screen is sequentially divided into the feed and initial threshing section, the fine threshing section, and the impurity discharge section. The lengths of these sections correspond to those of the front spiral feeder and rod-tooth section, the rear spike-tooth section, and the discharge section, respectively.

The curvature radius of the concave screen depends on the working radius of the drum and the threshing gap, and the geometric relationship is expressed as:

$$R_c = R_t + g \tag{5}$$

where, R_c is the curvature radius of the concave screen, R_t is the working radius of the drum and g is the threshing gap.

In this study, appropriately increasing the threshing gap in the feed and initial threshing section facilitates relatively free tumbling and unfolding of the ears as they enter the threshing zone, reduces feeding impact, and lowers the risk of kernel breakage. In contrast, reducing the threshing gap in the fine threshing and impurity removal sections is more conducive to thorough kneading and compression between the ears and the concave screen and teeth, thereby improving the completeness of kernel separation. A tapered transition structure is adopted to connect these two sections, allowing a smooth axial transition of ears from the feed and initial threshing stage to the fine threshing and impurity removal stage and avoiding material retention or accumulation caused by abrupt gap changes.

The upper guide cover plate is positioned above the threshing drum and, together with the concave screen, forms a closed and continuous threshing channel. Its primary function is to guide ear movement and regulate ear distribution. The cover plate is designed with an arched rigid structure to ensure structural strength and provide stable upper restraint for the material. A feed inlet is arranged at the front end of the cover plate and smoothly connected to the screw feeder to ensure uniform feeding of ears into the threshing area and prevent local material congestion.

To improve axial conveying performance, constant-pitch guide plates were arranged axially on the inner surface of the upper guide cover plate. These guide plates are inclined relative to the tangential direction of drum rotation. During operation, as the ears slide along the guide plates, they obtain a stable axial velocity component while being subjected to the tangential force generated by the drum. This relationship can be expressed by decomposing the drum tangential velocity into tangential and axial components, as shown in Eq. (6):

$$V_a = V_t \tan\alpha \tag{6}$$

Where V_t is the tangential velocity of the drum and α represents the inclination angle of the guide plate relative to the tangential direction. Based on cob dimensions and the observed material flow during testing, a relatively small guide angle was selected to achieve continuous axial conveyance and avoid cob bouncing or slipping.

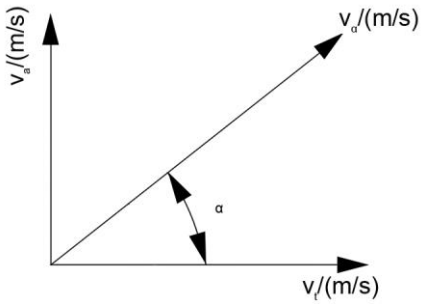

Fig. 4 - Schematic diagram of velocity decomposition on the guide cover plate

To visually demonstrate the effects of the concave plate screen and the upper guide cover plate during threshing, an EDEM simulation snapshot at a representative moment is shown in Fig. 5. The simulated material corresponds to experimental corn ears of the variety Xianyu 335. The DEM model employed representative physical parameters measured from the experimental material, including a density of 1200 kg/m³, a Poisson's ratio of 0.4, and a shear modulus of 1.37×10^8 Pa, with calibrated contact parameters. Figure 5 illustrates the distribution state of ears within the drum, their relative positions between the concave screen and the guide cover plate, and their axial movement trends. The simulation results show a clear overall conveying direction of the ears within the threshing channel, without material retention or disordered tumbling. This indicates that the combined constraint of the concave screen and the guiding effect of the cover plate ensure a stable axial conveying process *(Li et al., 2025)*.

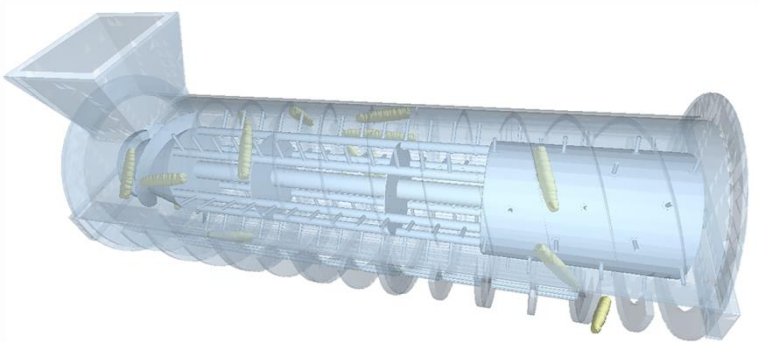

Fig. 5 - EDEM overall simulation result diagram

Dynamic Characteristics and Modal Safety Analysis of the Threshing Drum

In the combined axial-flow threshing unit, the threshing drum simultaneously performs ear agitation, kernel separation, and axial conveying. Therefore, the structural stiffness and dynamic response characteristics of the threshing drum have a significant influence on the operational stability of the entire machine. When rod teeth and spike teeth are arranged in series and multiple peripheral components are present, vibration amplification may occur if the natural frequency of the structure approaches the operating excitation frequency. This may disrupt the continuity of the threshing process and even threaten the structural reliability of the components. Consequently, it is necessary to conduct a verification analysis of the dynamic characteristics of the threshing drum after completion of the structural design *(Qu et al., 2018)*.

A three-dimensional model of the threshing drum was established in SolidWorks. While preserving the integrity of the main load-bearing components and structural features, bolts, chamfers, and other minor local details were appropriately simplified to avoid unnecessary interference with the modal analysis results. The simplified model was imported into the ANSYS Workbench platform in Parasolid format for modal analysis. The drum material was selected as 45 steel, and its elastic modulus, Poisson's ratio, and density were assigned according to standard engineering values.

Fixed boundary constraints were applied at the main shaft positions at both ends of the drum to simulate the constraint effects of bearings and support structures under actual assembly conditions. The first six natural frequencies and corresponding mode shapes were obtained using the Lanczos method, and the results are presented in Table 1. The results show that the first six natural frequencies of the combined axial-flow threshing drum range from 66.30 to 154.84 Hz, exhibiting a regular increasing trend with mode order and no frequency clustering or abnormal jumps.

Table 1

First six natural frequencies of the threshing drum

Order	Natural Frequency/Hz	Order	Natural Frequency/Hz
1	66.30	4	124.95
2	66.34	5	125.01
3	120.86	6	154.84

From the modal characteristics, the lower-order modes are mainly characterized by overall bending vibration of the drum, with the maximum deformation occurring at the mid-section of the drum and in the regions near the rod-tooth connecting pipes. As the modal order increases, the vibration gradually extends from overall bending to peripheral components, with increased participation of the rod-tooth pipes and the drum shell. In the higher-order modes, the end plate exhibits a certain disc-like bending behavior. It should be noted that the modal analysis results represent the relative deformation shapes of the structure at the corresponding natural frequencies and describe vibration modes rather than the actual vibration amplitudes under operating conditions. The modal shape contour plots for each order are shown in Fig. 6.

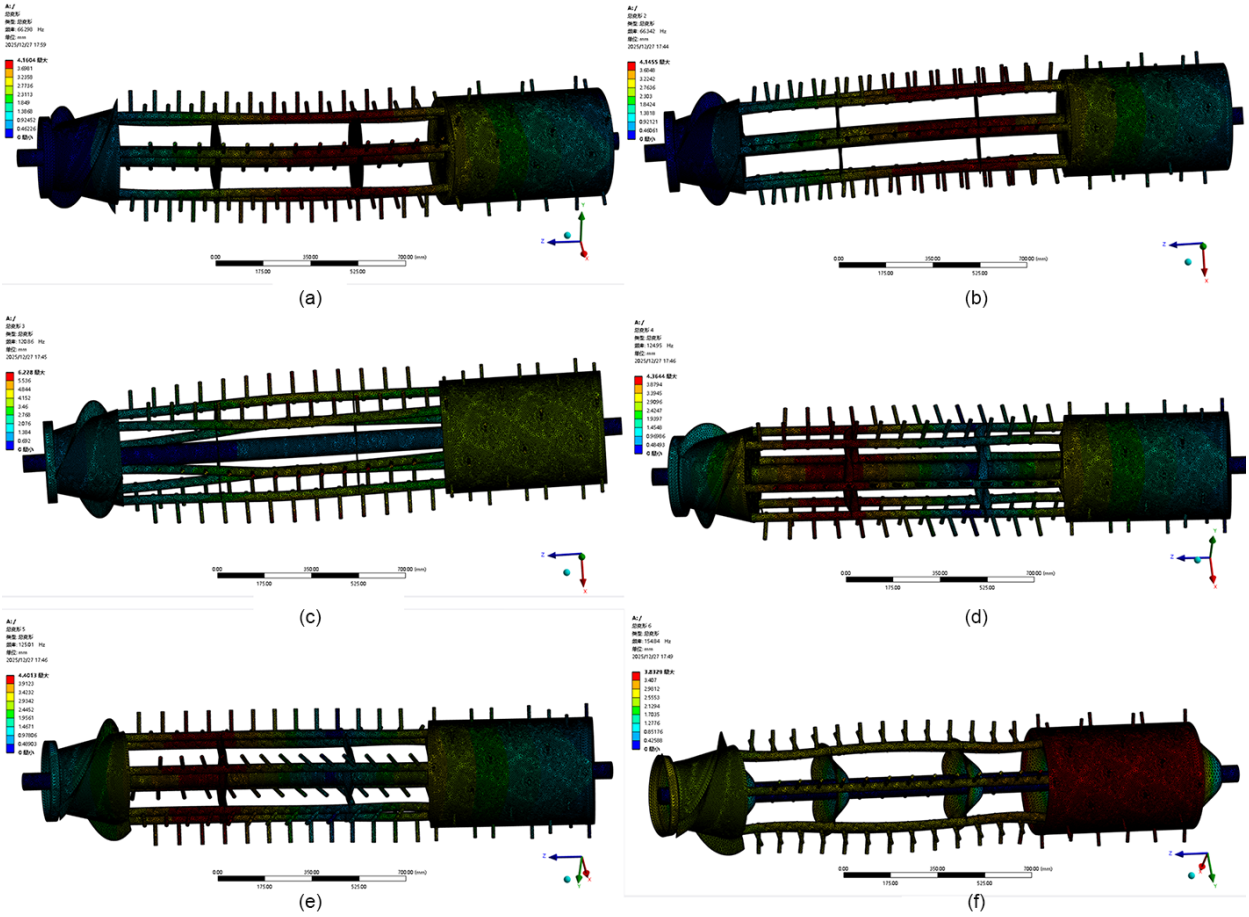

Fig. 6 - Modal shape contour maps of the combined threshing drum for each order

By combining the working parameters of the threshing device, the rotational excitation frequency of the drum can be determined. The relationship between the rotational excitation frequency and the drum rotational speed is expressed as Eq. (7):

$$f = \frac{n}{60} \tag{7}$$

where f denotes the rotational excitation frequency (Hz); N represents the drum rotational speed. Under normal operating conditions, the rotational excitation frequency corresponding to the drum speed is approximately 5 Hz, which is much lower than the first-order natural frequency. This indicates that the rotational excitation frequency is sufficiently separated from the natural frequencies of the system, satisfying the basic requirements of vibration-resistant mechanical design. Within this operating speed range, drum rotation is unlikely to excite the natural frequencies of the structure, thereby avoiding resonance and adverse effects on the threshing process and structural safety.

Experimental Materials

The corn ears used in the experiments were uniformly purchased by Qingdao Plantech Machinery Technology Co., Ltd. and were of the Xianyu 335 variety grown in North China. This variety has relatively large ears and moderate kernel adhesion, which helps ensure force stability within the threshing channel, reduces kernel damage caused by excessive compression, and is suitable for the structural design and performance testing of the combined axial-flow threshing device.

Experimental Method

The experiments were conducted in the workshop of the Qingdao Jiaozhou factory using a combined axial-flow corn threshing and separation device test bench. Before each test, a specified quantity of corn ears was smoothly fed into the inlet. The ears then entered the screw feeder, where ear feeding, kernel separation, and cob discharge were completed.

Fig. 7 - Modular axial-flow corn threshing and separation device test bench

Data collection and calculation during the tests were conducted using a high-precision electronic scale in accordance with GB/T 21962—2020 Corn Harvesting Machinery. The kernel breakage rate and incomplete threshing rate were selected as the main evaluation indicators. Each test group was repeated three times, and the average of the three measurements was taken as the final result.

Response Surface Design Plan and Results

To determine the optimal parameter combination, based on previous research results, drum speed, feed rate, and threshing gap were identified as the main influencing factors on threshing performance. Considering the kernel and ear characteristics of Xianyu 335, as well as the operational stability and damage control requirements of the threshing device, the drum speed range was set to 250-350 r/min, the feed rate range to 3.0-5.0 kg/s, and the threshing gap range to 35-45 mm.

Using Design-Expert 10.0 software, a Box-Behnken response surface design with three factors and three levels was established. The kernel breakage rate (Y_1) and unthreshed kernel rate (Y_2) were selected as response variables to analyze the effects of multiple factors and their interactions. Five replicates were set at the center point, resulting in a total of 17 experimental runs to reduce systematic error and improve model reliability. Each factor was coded according to its level, as shown in Table 2.

Table 2

Level coding table

Coding Value	Level		
	Drum Speed / (r/min)	Feed Rate / (kg/s)	Threshing Gap / (mm)
-1	250	3.0	35
0	300	4.0	40
1	350	5.0	45

RESULTS

The experimental design and corresponding results are presented in Table 3.

Table 3

Box-Behnken test protocol and results

Experiment No.	Experimental Factor			Experimental Indicator	
	A	B	C	Kernel Breakage Rate Y_1 /%	Unthreshed Rate Y_2 /%
1	0	0	0	3.85	0.47
2	-1	0	1	3.78	0.65
3	0	-1	-1	4.87	0.40
4	0	1	1	3.03	0.54
5	0	0	0	3.55	0.48
6	1	0	1	3.25	0.35
7	1	1	0	4.62	0.33
8	-1	1	0	3.72	0.62
9	1	-1	0	3.52	0.36
10	-1	0	-1	4.15	0.68
11	0	0	0	3.91	0.42
12	0	-1	1	4.31	0.60
13	0	0	0	4.28	0.46
14	-1	-1	0	3.65	0.66
15	0	1	-1	3.48	0.43
16	0	0	0	3.38	0.52
17	1	0	-1	3.60	0.34

ANOVA for Experimental Results

Based on the experimental data presented in Table 3, Design-Expert 10.0 software was used to establish a quadratic polynomial regression model describing the relationships between the kernel breakage rate, unthreshed kernel rate, and the experimental factors.

$$Y_1 = 3.790 - 0.039A - 0.190B - 0.220C + 0.260AB + 0.005AC + 0.028BC - 0.072A^2 + 0.160B^2 - 0.027C^2 \quad (8)$$

$$Y_2 = 0.470 - 0.150A - 0.012B + 0.036C + 0.003AB + 0.010AC - 0.022BC + 0.018A^2 + 0.005B^2 + 0.018C^2 \quad (9)$$

As shown in Tables 4 and 5, the regression models for kernel breakage rate and unthreshed kernel rate differ in their levels of significance. The regression model for unthreshed kernel rate yielded P=0.0054, reaching a highly significant level (P<0.01), indicating that the established quadratic regression model can effectively describe the effects of drum speed, feed rate, and threshing gap on the unthreshed kernel rate. Although the overall significance of the kernel breakage rate model was relatively low, the P value of the lack-of-fit term was greater than 0.05, indicating no significant lack of fit; therefore, the model still exhibits acceptable fitting reliability within the tested parameter range.

In terms of factor effects, neither the main effects nor the interaction effects in the kernel breakage rate model reached statistical significance (P>0.05). This indicates that variations in kernel breakage rate were relatively small within the selected parameter ranges, suggesting that the combined axial-flow threshing structure provides a favorable cushioning effect on kernels. In the unthreshed kernel rate model, drum speed (A) had an extremely significant effect (P<0.0001, F=68.50) and was the dominant factor, while threshing gap (C) had a moderate influence and feed rate (B) had a relatively minor effect. The interaction and quadratic terms were not significant in either model, indicating that no pronounced nonlinear or abrupt changes in response values occurred within the investigated parameter range.

Table 4

Variance analysis (ANOVA) of the quadratic polynomial model for kernel breakage rate

Source	Sum of Squares	Degrees of Freedom	Mean Square	F Value	P Value
Model	1.06	9	0.12	0.30	0.952 8
A	0.012	1	0.012	0.030	0.866 5

Source	Sum of Squares	Degrees of Freedom	Mean Square	F Value	P Value
B	0.28	1	0.28	0.71	0.426 7
C	0.37	1	0.37	0.95	0.362 9
AB	0.27	1	0.27	0.67	0.439 6
AC	1.00×10^{-4}	1	1.00×10^{-4}	2.53×10^{-4}	0.987 7
BC	3.03×10^{-3}	1	3.03×10^{-3}	7.66×10^{-3}	0.932 7
A^2	0.022	1	0.022	0.055	0.820 9
B^2	0.10	1	0.10	0.26	0.627 3
C^2	3.07×10^{-3}	1	3.07×10^{-3}	7.77×10^{-3}	0.932 2
Residual	2.77	7	0.40		
Lack of fit	2.28	3	0.76	6.29	0.053 9
Error	0.48	4	0.12		
Sum	3.82	16			

Table 5

Variance analysis (ANOVA) of the second-order polynomial model for unthreshed kernel rate

Source	Sum of Squares	Degrees of Freedom	Mean Square	F Value	P Value
Model	0.21	9	0.023	8.30	0.005 4**
A	0.19	1	0.19	68.50	<0.000 1**
B	1.25×10^{-3}	1	1.25×10^{-3}	0.45	0.522 6
C	0.01	1	0.01	3.81	0.092 0
AB	2.50×10^{-5}	1	2.50×10^{-5}	9.06×10^{-3}	0.926 9
AC	4.00×10^{-4}	1	4.00×10^{-4}	0.14	0.714 8
BC	2.03×10^{-3}	1	2.03×10^{-3}	0.73	0.420 1
A^2	1.29×10^{-3}	1	1.29×10^{-3}	0.47	0.516 3
B^2	1.05×10^{-4}	1	1.05×10^{-4}	0.04	0.850 7
C^2	1.29×10^{-3}	1	1.29×10^{-3}	0.47	0.516 3
Residual	0.019	7	2.76×10^{-3}		
Lack of fit	0.014	3	4.71×10^{-3}	3.62	0.122 9
Error	5.20×10^{-3}	4	1.30×10^{-3}		
Sum	0.23	16			

Response Surface Analysis

Using Design-Expert 10.0 software, quadratic regression models were established to construct three-dimensional response surfaces of the kernel breakage rate and unthreshed kernel rate under the pairwise interactions of drum speed (A), feed rate (B), and threshing gap (C), as shown in Figs. 8(a) - (f).

From Figs. 8(a)-8(c), it can be observed that within the selected parameter ranges, the combined effects of the factors on kernel breakage rate were generally moderate. The response surfaces are relatively smooth, with no obvious extreme regions, indicating the absence of significant three-factor interactions, which is consistent with the ANOVA results. Appropriately increasing the threshing gap can reduce kernel compression and impact, thereby lowering the kernel breakage rate.

As shown in Figs. 8(d)-8(f), the unthreshed kernel rate is more sensitive to variations in drum speed. With increasing drum speed, threshing effectiveness improves, resulting in a decreasing trend in the unthreshed kernel rate. An excessively large threshing gap leads to an increase in the unthreshed kernel rate, while the influence of feed rate is relatively weak. Overall, the results indicate that each factor mainly affects threshing performance independently, and the combined axial-flow threshing device operates stably within the investigated parameter ranges.

Experimental Optimization

To determine the optimal operating parameter combination of the threshing device under multiple factors, multi-objective nonlinear optimization was carried out using Design-Expert 10.0 software based on the significance analysis results of the above regression models. With the objectives of minimizing the kernel breakage rate and unthreshed kernel rate, drum speed, feed rate, and threshing gap were selected as independent variables, with ranges of 250 ~ 350 r / min, 3.0 ~ 5.0 kg / s, and 35 ~ 45 mm, respectively. By integrating the response surface regression equations, a nonlinear performance model of the threshing device was established as follows:

$$\begin{cases} min\, Y_1 \\ min\, Y_2 \\ s.t. \begin{cases} 250\ r/min \le A \le 350\ \mathrm{r/min} \\ 3.0 kg/s \le B \le 5.0\ \mathrm{kg/s} \\ 35 mm \le C \le 45\ \mathrm{mm} \end{cases} \end{cases} \quad (10)$$

Using the optimization function of the software, an optimal solution with a comprehensive desirability of 1 was obtained. Under this condition, the optimal drum speed was 339.017 r/min, the feed rate was 3.642 kg/s, and the threshing gap was 44.984 mm, corresponding to a kernel breakage rate of 3.487% and an unthreshed kernel rate of 0.434%. The optimization results indicate that the model exhibits good convergence and prediction reliability, and the obtained optimal parameter combination effectively balances threshing efficiency and kernel damage control.

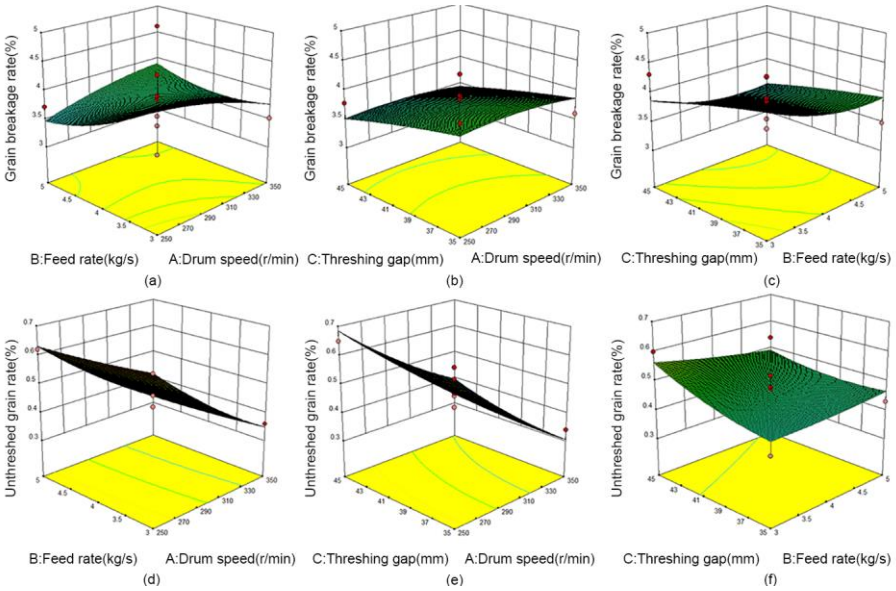

Fig. 8 - Response surface plots showing the effects of factor interactions

Field Validation Trial

To verify the effectiveness and practicality of the parameter combination obtained from response surface optimization, field validation tests were conducted at Qingdao Agricultural University. Based on the multi-objective optimization results, the validation parameter combination was selected as a drum speed of 339 r/min, a feed rate of 3.6 kg/s, and a threshing gap of 45 mm. The operating conditions were consistent with those used in the previous experiments, and material feeding and conveying were carried out using a combine harvester. The kernel breakage rate and unthreshed kernel rate were measured as performance indicators. Each test was repeated three times, with approximately 15 kg of samples collected per test, and the average values were taken as the final results.

As shown in Table 6, the kernel breakage rates of the three trials were 3.66%, 4.02%, and 3.87%, with an average value of 3.850%. The unthreshed kernel rates were 0.41%, 0.52%, and 0.49%, with an average value of 0.473%. Compared with the values predicted by the Design-Expert model (kernel breakage rate of 3.487% and unthreshed kernel rate of 0.434%), the relative errors of both indicators were within acceptable engineering tolerance ranges, indicating good agreement between model predictions and experimental results.

Table 6

Field trial results

Trial Group	Kernel Breakage Rate Y_1 /%	Unthreshed Kernel Rate Y_2 /%
1	3.66	0.41
2	4.02	0.52
3	3.87	0.49
Average	3.850	0.473

During field operation, the threshing mechanism operated smoothly, with complete kernel separation and unobstructed cob discharge, without congestion or blockage. The test results show that under optimized parameters, the device achieves a low kernel breakage rate and a high threshing efficiency, meeting the technical requirements of GB/T 21962-2020 Corn Harvesting Machinery (kernel breakage rate ≤5%, unthreshed kernel rate ≤4%). These results further demonstrate the reliability of the model and the feasibility of the optimized parameter combination.

CONCLUSIONS

(1) To meet the operational requirements of reducing kernel damage and improving threshing efficiency in corn plot harvesting, a combined rod-tooth/spike-tooth axial-flow threshing structure was developed. By introducing a segmented threshing mechanism along the axial direction of the drum, corn ears are sufficiently agitated and preliminarily threshed before entering the high-intensity threshing section. This staged structural design effectively avoids stress concentration during initial threshing, thereby reducing the risk of excessive kernel breakage.

(2) Threshing elements were arranged in a spiral configuration in combination with a guiding structure to enhance axial ear movement within the drum. Discrete element simulation results show significant axial velocity fluctuations in the rod-tooth section, while the motion becomes stable after entering the spike-tooth section. The transition from turbulent transport to continuous axial conveying confirms that the combined structure improves the continuity of axial movement.

(3) A closed threshing channel was formed using a segmented concave plate screen and an upper guide cover plate equipped with spiral guide plates, providing matched constraint and guidance conditions for ears at different threshing stages. EDEM simulation results show that ears are uniformly distributed within the threshing channel, exhibiting a clear axial movement direction without significant retention or disordered tumbling. This demonstrates that the concave screen and guide cover plate achieve effective synergistic performance during axial threshing.

(4) Finite element modal analysis was conducted to evaluate the dynamic characteristics of the threshing drum. The results indicate that the first six natural frequencies of the drum are significantly higher than the rotational excitation frequency under normal operating speeds. The mode shapes are mainly characterized by overall bending and localized component vibrations, confirming that the threshing drum exhibits good dynamic structural safety during operation.

(5) A Box-Behnken response surface experiment was conducted to establish a regression model linking operating parameters with threshing performance. The analysis shows that drum speed has a significant effect on the unthreshed kernel rate, while the kernel breakage rate varies only slightly within the selected parameter range, indicating that the combined axial-flow threshing structure provides effective cushioning and damage reduction for kernels. The optimal operating parameter combination was determined as a drum speed of approximately 339 r/min, a feed rate of about 3.6 kg/s, and a threshing gap of around 45 mm. Field validation tests showed a kernel breakage rate of 3.85% and an unthreshed kernel rate of 0.47%, which are consistent with the model predictions.

ACKNOWLEDGEMENT

This research was supported by the National Key Research and Development Program of China through the project *"Research and Development of Intelligent Harvesting Technology and Equipment for Low-Loss and High-Cleanliness Seed Production of Kernel Crops"* (No. 2023YED2000404).

REFERENCES

[1] Abdeen M.A., Salem A.E., Zhang G., (2021). Longitudinal axial flow rice thresher performance optimization using the Taguchi technique. *Agriculture,* 11, pp. 88–102. DOI: https://doi.org/10.3390/agriculture11020088

[2] Chen Y., (2024). Current situation and development trend of corn harvesting machinery (玉米收获机械的现状及发展趋势). *Seed Technology*, 42(12), pp. 142–144.

[3] Chen Z., Wassgren C., Ambrose R.P.K., (2021). Measured damage resistance of corn and wheat kernels to compression, friction, and repeated impacts. *Powder Technology*, 380, pp. 638–648. DOI: https://doi.org/10.1016/j.powtec.2020.11.060

[4] Di Z.F., Cui Z.K., Zhang H., Zhou J., Zhang M.Y., Bu L.X., (2018). Design and experiment of an axial-flow corn threshing drum combined with rasp bar blocks and spike teeth (纹杆块与钉齿组合式轴流玉米脱粒滚筒的设计与试验). *Transactions of the Chinese Society of Agricultural Engineering*, 34(1), pp. 28–34. DOI: https://doi.org/10.11975/j.issn.1002-6819.2018.01.004

[5] Li L., Zhou Y., Nie J., Li Q., Zhang L., (2025). Optimization design of tangential flow–transverse axial flow double-drum maize threshing device based on EDEM. *INMATEH Agricultural Engineering*, 77, pp. 647–662. DOI: https://doi.org/10.35633/inmateh-77-53

[6] Li X.R., Mao X., Yi S.J., Wang X., Chen T., Wang S.H., (2024). Design and experiment of plate-tooth axial-flow corn threshing and separating device (板齿式轴流玉米脱粒分离装置设计与试验). *Journal of Chinese Agricultural Mechanization*, 45(11), pp. 106–112, 130.

[7] Mousaviraad M., Tekeste M.Z., (2020). Effect of grain moisture content on physical, mechanical, and bulk dynamic behaviour of maize. *Biosystems Engineering*, 195, pp. 186–197. DOI: https://doi.org/10.1016/j.biosystemseng.2020.04.012

[8] Qu Z., Zhang D.X., Yang L., Zhang T.L., Wang Z.D., Cui T., (2018). Feeding rate and drum speed experiment of longitudinal axial-flow corn threshing and separating device (纵轴流玉米脱粒分离装置喂入量与滚筒转速试验). *Transactions of the Chinese Society for Agricultural Machinery*, 49(2), pp. 58–65.

[9] Shi B., (2018). *Design and experiment of rasp-bar corn ear threshing device* (纹杆式玉米种穗脱粒装置的设计与试验). *MSc Thesis*, Sichuan Agricultural University, Ya'an/China. DOI: https://doi.org/10.27345/d.cnki.gsnyu.2018.000191

[10] Shi H.Y., Alimu M.M.T.X., Xu Y.L., Zhang J.S., Li Q.X., Che T., (2025). Design and experiment of double longitudinal axial-flow threshing device for corn grain harvester (玉米籽粒收获机双纵轴流脱粒装置设计与试验). *Journal of Agricultural Mechanization Research*, 47(12), pp. 166–175.

[11] Srison W., Chuan-Udom S., Saengprachatanarak K., (2016). Effects of operating factors for an axial-flow corn shelling unit on losses and power consumption. *Agriculture and Natural Resources*, 50(5), pp. 421–425.

[12] Steponavičius D., Kemzūraitė A., Pužauskas E., Domeika R., Grigas A., Karalius D., (2023). Shape optimization of concave crossbars to increase threshing performance of moist corn ears. *Agriculture*, 13, pp. 983–1003. DOI: https://doi.org/10.3390/agriculture13050983

[13] Vladut N.-V., Biris S.-S., Cardei P., Gageanu I., Cujbescu D., Ungureanu N., Popa L.-D., Perisoara L., Matei G., Teliban G.-C., (2022). Contributions to the mathematical modeling of the threshing and separation process in an axial flow combine. *Agriculture*, 12, 1520. DOI: https://doi.org/10.3390/agriculture12101520

[14] Vladut N.-V., Ungureanu N., Biris S.-S., Voicea I., Nenciu F., Gageanu I., Cujbescu D., Popa L.-D., Boruz S., Matei G., Ekielski A., Teliban G.-C., (2023). Research on the identification of some optimal threshing and separation regimes in the axial flow apparatus. *Agriculture*, 13, pp. 838–855. DOI: https://doi.org/10.3390/agriculture13040838

[15] Wang Z.D., Cui T., Zhang D.X., Yang L., He X.T., Zhang Z.P., (2021). Design and experiment of rasp-bar threshing element for corn combine harvester (玉米联合收获机纹杆式脱粒元件设计与试验). *Transactions of the Chinese Society for Agricultural Machinery*, 52(9), pp. 115–123.

[16] Xin S.L., Zhao W.Y., Qu H., Yang T., Shi R.J., Yan Z.B., Ma H.J., (2024). Review and development trend of mechanized corn harvesting technology (玉米机械化收获技术现状分析及发展趋势). *Journal of Agricultural Mechanization Research*, 46(10), pp. 9–14.

[17] Xing S., Cui T., Zhang D., Yang L., He X., Li C., Dong J., Jiang Y., Wu W., Zhang C., Du Z., (2024) Design and optimization for a longitudinal-flow corn ear threshing device of low loss and low energy consumption. *Computers and Electronics in Agriculture*, 226, 109328. DOI: https://doi.org/10.1016/j.compag.2024.109328

[18] Yuan L., He X., Zhu C., Wang W., Wang M., Wu S., (2024). Design and test of tangential and longitudinal-axial threshing and separating unit for wheat. *Results in Engineering*, 21, 101774. DOI: https://doi.org/10.1016/j.rineng.2024.101774

[19] Zhang J., Zhao L., Yi S., Zhang D., Zhang X., (2025). Establishment and validation of a theoretical model for single longitudinal axial flow threshing and separation of millet. *INMATEH Agricultural Engineering*, 76, pp. 100–110. DOI: https://doi.org/10.35633/inmateh-76-09

[20] Zhao D.H., Narisu, Wu D.W., (2024). Development status and suggestions of loss reduction technology for corn mechanized harvesting (玉米机械化收获减损技术发展现状与建议). *China Agricultural Machinery Equipment*, (8), pp. 23–26.